A98-31501 ICAS-98-2,3,4

A SIMPLE WING OPTIMIZATION CODE INCLUDING PROPELLER EFFECTS

L.L.M. Veldhuis, P.M. Heyma
Delft University of Technology, Dept. of Aerospace Engineering
Low Speed Aerodynamics Laboratory
Leeghwaterstr. 42, 2628 CA Delft, the Netherlands

Abstract

To further analyze the possibilities of optimized designs a simple and fast calculation method for optimal lift distributions of tractor propeller/wing configurations is formulated and discussed. The optimization algorithm is based on a Trefftz-plane analysis where the conservation laws of mass, momentum and energy are fulfilled in a control volume surrounding the configuration.
The paper discusses the formulation of the optimization algorithm based on augmented Lagrange integrals. The effect of viscous effects is incorporated in the calculation process. The method described above was implemented in a computer program which enables the user find the optimum lift distribution for minimum drag for any tractor propeller / wing arrangement of arbitrary shape. As input for the slipstream data the user can either select input of experimental data or generate artificial data using a simple slipstream model based on the well known blade element theory with Prandtl tip loss factor. Some numerical studies, show that optimization of a modern medium speed turboprop aircraft (Fokker-50-like configuration) leads to performance increase by adapting the wing geometry and twist distribution.

Symbols

A	wing aspect ratio
b	wing span
c	local chord
C	intersection curve in the Trefftz plane
c_d	local drag coefficient
c_l	local lift coefficient
C_L	total lift coefficient of the configuration
C_N	normal force coefficient
D	drag force, propeller diameter
e	span efficiency factor
H	total pressure
$\overline{n}$	normal vector
p	pressure
P	power
Q	torque
S	wing area
T	thrust force, temperature
U_0	undisturbed flow velocity
u, v, w	x,y and z-component of the velocity vector
$\overline{U}$	average flow velocity
v_a	axial velocity increase in the slipstream
v_t	tangential velocity increase in the slipstream
x, y, z	coordinates in streamwise, spanwise and vertical direction respectively
α_g	geometrical angle of attack
α_0	zero lift angle of attack
α_i	induced angle of attack
ρ	air density
Γ	bound circulation strength
ς	local dihedral angle
η	dimensionless spanwise coordinate
ω	propeller rotational speed

Indices

c.l.	center line
i	induced
opt	optimum
p	propeller
ref	reference value
v	viscous
w	wing

Introduction

In the design of multi-engined propeller powered aircraft one of the important points of concern is the interaction between the propeller slipstream and the wing. Modern aircraft concepts, like the European FLA project exhibit high disk loading and an increased number of (swept) blades to enable high cruising speed. The generation of strong swirl velocities in the slipstream however generate a considerable deformation of the lift distribution which has an impact on the aerodynamic behavior and performance of the wing. From earlier investigations it is known that both the position of the powerplant with respect to the wing and propeller angle of attack play an important role. Carefully designed configurations may reveal some performance benefits when the propeller and the wing are closely coupled.

Although the rotational kinetic energy in the wake of the conventional single-rotating propulsion systems

is usually lost and does not contribute to the thrust. analyses by Kroo[1] , Miranda[2] and Veldhuis[3] have indicated that significant wing drag reduction can be obtained for propeller / wing interaction. Rather than manipulate wing geometry to approach two-dimensional flow, it would seem logical to use some energy source for the task of directing the flow such that lower induced drag is produced. Although the rotational component in the slipstream always has been considered to represent lost energy it is in fact available for amplifying or attenuating the wing vortex with a possible reduction of induced drag. In fact the wing acts as a stator vane that recovers some of the swirl loss caused by the propeller.

To derive a better understanding of the interactive flows causing the slipstream/wing interference an optimization program was developed in which the slipstream velocity effects are incorporated.
The phenomena that play a role with respect to the interaction between the propeller and the wing have been described by Kroo[1], Heyma[5] and Veldhuis[3] and many others. In the subsequent paragraphs a description will be given of the optimization program.

Theoretical approach

Introduction

In the last decade CFD programs have become available in which the interaction of propeller and wing can be analyzed based on a solution of the Navier-Stokes equations[7,8]. Although the results of these codes contribute without doubt to a better understanding of the problem of propulsion integration generally they lack one important feature : an optimization algorithm. Optimization programs are very important in the preliminary design phase when the main design parameters like the location of the propulsion system have to be chosen. Since these methods should be fast enough to quickly access the consequences of changes in the global shape of the configuration they are often based on elementary momentum considerations and relatively simple numerical schemes. In the following paragraphs the theoretical approach which is the basis for the optimization program *pwopt2* is described.

Drag Breakdown

In case the drag is to be minimized for a given lift coefficient it is important to distinguish the various contributions as found from a phenomenological approach :

- body minimum drag in absence of lift
- drag due to lift
- compressibility drag
- trim drag
- miscellaneous drag due to interference effects and excrescencies.

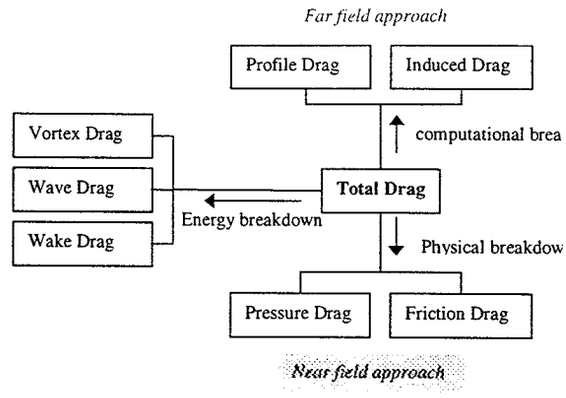

fig. 1 Methods for drag breakdown as proposed by Middel[9].

Because the interactions between the different phenomena is very complex an independent determination of the drag components is generally not possible. As stated by Middel[9] the drag can be considered in 3 different ways (fig. 1) based on :

- the nature of the elementary forces (physical breakdown)
- the (non) lift generated sources (far field approach)
- the energy losses in the flow field (energy breakdown)

The drag breakdown in elementary forces leads to pressure drag and friction drag which can, for example be calculated by an inviscid code and a boundary layer code respectively. The near field approach may lead however to considerable errors due to discretization of the geometry (inaccurate integration of surface forces).
The breakdown into (non)lift related sources leads to induced drag and profile drag. The induced drag , which arises due to the generation of normal forces by the lifting surfaces, can be calculated with the so-called Trefftz plane analysis[9]. Because the far field approach is based on the analysis of the circulation distribution in the far wake it requires a less detailed geometry description than the near field approach. Therefore it is often the preferred method while investigating the global characteristics of the aircraft in the design phase.
The breakdown into the energy losses leads to the vortex drag, the wake drag and the wave drag.

In our analysis the so-called Trefftz plane method is applied to the propeller wing configuration.
The method, based on Munk's stagger theorem[10], was originally applied to wing tail configurations but may be extended to propeller-wing configurations as well, as indicated by Kroo[1].
Initially the influence of the wing on the propeller is neglected which implies that the propeller is far upstream or downstream of the wing.

Hence the total downwash at infinity, used in the optimization process, is a superposition of the downwash due to all lifting surfaces and the downwash generated by the propeller at infinity.

Drag minimization

To optimize the performance of the propeller-wing configuration the drag at a given lift in minimized. In our case this leads to the following successive steps :

- the choice of the drag function to be optimized
- the choice of independent variables
- the calculation of the drag for each configuration
- the calculation of the drag for each combination of the independent variables
- the choice of the constraint function
- the optimization algorithm

The inverse numerical optimization applied here is based on a relatively simple flow solver which utilizes a lifting line theory to model the lifting surfaces combined with a Trefftz plane analysis. The bound circulation is modeled quadratic similar to the method of Kuhlman[4].
Examples of comparable optimization codes were already described by Miranda & Brennan[2], Kroo[1] and Veldhuis[3].
These approaches differ from the current analysis in the way the lift distribution is modeled. The above stated authors, for example proposed a modeling technique incorporating Fourier sine series combined with axial and tangential velocities induced by the propellers.

The drag can be calculated by considering the momentum balance of a control surface S which surrounds the configuration (fig. (2)).
A detailed mathematical description of the lift and the drag analysis is beyond the scope of this paper. Therefore only the most important calculation and derivation results will be summarized here.
A more detailed analysis is presented by Van den Dam[11], Middel[9], Heyma[5] and Veldhuis[3].
In the following analysis the effects of compressibility will be neglected since most propeller aircraft operate in the (low) subsonic speed regime.

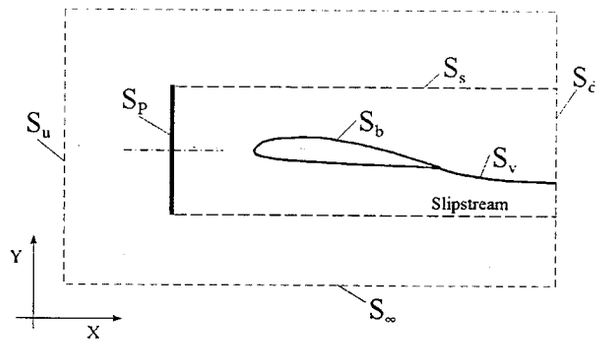

fig. 2 Layout of the control volume and the control surface as used in the Trefftz analysis

Trefftz plane analysis

When the basic equations of conservation of mass, momentum and energy are applied to the control volume S in x-direction we may write :

$$\begin{aligned} &\int_S \rho(\overline{U}\cdot\overline{n})dS = 0 \\ &\int_S (p\,n_x + \rho u(\overline{U}\cdot\overline{n}))dS = 0 \\ &\int_S \rho H(\overline{U}\cdot\overline{n})dS = 0 \end{aligned} \qquad (1)$$

Here the control surface S is build up of several subsurface : $S = S_u + S_\infty + S_d + S_v + S_p + S_s$

Since for the moment the viscous forces are neglected the only resulting force in x-direction will be the induced drag. Hence the surface integral can be simplified to :

$$\begin{aligned} 0 &= \int_{S_u+S_d} \rho(\overline{U}\cdot\overline{n})dS \\ D_i &= -\int_{S_u+S_d+S_p} (p\,n_x + \rho u(\overline{U}\cdot\overline{n}))dS \\ 0 &= \int_{S_u+S_d+S_p} \rho H(\overline{U}\cdot\overline{n})dS \end{aligned} \qquad (2)$$

Energy conservation over the propeller disk results in:

$$\int_{S_p} \rho H\left(\overline{U}\cdot\overline{n}\right)dS = -U_\infty T - \omega Q \qquad (3)$$

here U_∞ is the free steam velocity, T is the thrust and Q the torque of the propeller.
The propeller thrust is defined by :

$$T = \int_{S_p} \left(pn_x + \rho u\left(\overline{U}\cdot\overline{n}\right)\right)dS \qquad (4)$$

Combining the above equations and introducing the velocity potential Φ the induced drag can be written as :

$$D_i = -\int_{S_U+S_D} \left(pn_x + \rho\frac{d\Phi}{dx}(\nabla\Phi\cdot\bar{n}) - \rho\frac{H}{U_\infty}(\nabla\Phi\cdot\bar{n})\right)dS - \frac{\omega Q}{U_\infty} \qquad (5)$$

Now the isentropic relation for pressure and density is introduced :

$$\frac{p}{p_\infty}=\left[\frac{\rho}{\rho_\infty}\right]^\gamma$$
$$=\left[1-(\frac{\gamma-1}{2})M_\infty^2\left(\frac{\varphi'-2\Delta H}{U_\infty^2}-1\right)\right]^{\frac{\gamma}{\gamma-1}} \quad (6)$$

where $\varphi'=(U_\infty+\frac{\partial\varphi}{\partial x})^2+(\frac{\partial\varphi}{\partial y})^2+(\frac{\partial\varphi}{\partial z})^2$

Here $\frac{\partial\varphi}{\partial x},\frac{\partial\varphi}{\partial y},\frac{\partial\varphi}{\partial z}$ are the perturbation velocities while ΔH is the change in total enthalpy.

Assuming the perturbation velocities are small eq. (6) can be approximated by a Taylor expansion. This results in :

$$D_i=-\rho_\infty\int_{S_u+S_d}(\left(\frac{1}{\gamma}\frac{U_\infty^2}{M_\infty^2}\right)-\frac{1}{2}\left(\left(\frac{\partial\varphi}{\partial x}\right)^2+\left(\frac{\partial\varphi}{\partial y}\right)^2+\left(\frac{\partial\varphi}{\partial z}\right)^2\right)n_x+(\frac{\partial\Phi}{\partial x})(\nabla\Phi\cdot\bar{n})-\frac{H}{U_\infty}(1-\frac{U_\infty^2}{M_\infty^2}\left(\left(\frac{\partial\varphi}{\partial x}\right)^2+\left(\frac{\partial\varphi}{\partial y}\right)^2+\left(\frac{\partial\varphi}{\partial z}\right)^2\right)\cdot(\nabla\Phi\cdot\bar{n})+O(\varepsilon^3))dS-\frac{\omega Q}{U_\infty} \quad (7)$$

Far upstream the perturbation integrals vanish hence only the integration far downstream (Trefftz plane) remains. With $\Delta H=H-H_\infty\approx U_\infty(\partial\varphi/\partial x)$ the resulting Trefftz plane integral becomes :

$$D_i=\frac{\rho_\infty}{2}\int_{S_T}\left((\frac{\partial\varphi}{\partial x})^2+(\frac{\partial\varphi}{\partial x})^2+(\frac{\partial\varphi}{\partial x})^2\right)-\frac{\omega Q}{U_\infty} \quad (8)$$

The perturbation φ is build up of a disturbance due to the wing/body (index b) and the potential due to the propeller (index p).

Neglecting $\partial\varphi_b/\partial x$ (the flow is fully "developed"), the induced drag becomes :

$$D_i=\frac{\rho_\infty}{2}\int_{S_T}(\partial\varphi_{b_y}{}^2+\partial\varphi_{b_z}{}^2)\,dS+\rho_\infty\int_{S_T}(\partial\varphi_{b_y}\partial\varphi_{p_y}+\partial\varphi_{b_z}\partial\varphi_{p_z})\,dS+\frac{\rho_\infty}{2}\int_{S_T}(\partial\varphi_{p_x}{}^2+\partial\varphi_{p_y}{}^2+\partial\varphi_{p_z}{}^2)\,dS-\frac{\omega Q}{U_\infty} \quad (9)$$

Using Green's identity the integral over S is transformed into an integral over the intersection curve(s) C_T formed by the intersection of the wake and the Trefftz plane. The first integral of eq. (9) is rewritten in the form :

$$\int_{S_T}\left((\frac{\partial\varphi}{\partial y})^2+(\frac{\partial\varphi}{\partial z})^2\right)dS=\int_{C_T}\frac{\partial\varphi}{\partial n}\varphi\,dC-\int_{S_T}\varphi\left(\frac{\partial^2\varphi}{\partial y^2}+\frac{\partial^2\varphi}{\partial z^2}\right)dS \quad (10)$$

while the second integral becomes :

$$\int_{S_T}(\bar{U}_p\cdot\nabla\varphi_b)dS=\int_{C_T}\varphi(\bar{U}_p\cdot\bar{n})dC-\int_{S_T}\varphi\left(\frac{\partial v_p}{\partial y}+\frac{\partial w_p}{\partial z}\right)dS \quad (11)$$

where $\bar{U}_p=(\frac{\partial\varphi_p}{\partial x},\frac{\partial\varphi_p}{\partial y},\frac{\partial\varphi_p}{\partial z})$ is the velocity vector induced by the propeller.

At the Trefftz plane both the second terms in eq. (10) and (11) vanish.
The jump in the velocity across the wake is equivalent to the local circulation. Hence with $\Delta\varphi=\Gamma$ and $\partial\varphi/\partial n=v_n$ the induced drag in the Trefftz plane becomes :

$$D_i = \frac{\rho_\infty}{2} \int_{C_T} \Gamma\left(v_n + 2(v_P \cdot n_y + w_P \cdot n_z)\right) dC + \frac{\rho_\infty}{2} \int_{S_P} \left(u_P^2 + v_P^2 + w_P^2\right) dS - \frac{\omega Q}{U_\infty} \quad (12)$$

Three terms can be distinguished :

$$A = \frac{\rho_\infty}{2} \int_{C_T} v_n \Gamma \, dC \quad (13)$$

the induced drag without the presence of a slipstream

$$B = \rho_\infty \int_{C_T} \Gamma\left(v_P \cdot n_y + w_P \cdot n_z\right) dC = \rho_\infty \int_{C_T} \Gamma \, v_{n_p} \, dC \quad (14)$$

the propeller-wing interaction effect

$$C = \frac{\rho_\infty}{2} \int_{S_P} \left(u_P^2 + v_P^2 + w_P^2\right) dS - \frac{\omega Q}{U_\infty} \quad (15)$$

the "swirl loss" of the propeller.

Now eq. (12) can be written as a drag coefficient :

$$C_{D_i} = \frac{1}{U_\infty^2 S_{ref}} \int_{C_T} \Gamma (v_n + 2(v_p \cdot n_y + w_p \cdot n_z)) dC + \sum_{i=1}^{n_p} C_i^* \quad (16)$$

with :

$$C_i^* = \frac{1}{U_\infty^2 S_{ref}} \int_{S_P} \left(u_P^2 + v_P^2 + w_P^2\right) dS - \frac{1}{2\rho_\infty U_\infty^2 S_{ref}} \frac{1}{\lambda_i} \left(\frac{Q}{D}\right)_i \quad (17)$$

Without further proof it is stated that in an analogue way for the lift coefficient the following relation can be derived :

$$C_L = \frac{2}{U_\infty^2 S_{ref}} \int_{C_T} \Gamma\left(\left(U_\infty + u_p\right) \cos\zeta\right) dC \quad (18)$$

where u_p is the axial velocity increase due to the propeller and ζ is the wing dihedral.

Viscous drag

An optimization in which only the induced drag is minimized may result in a lift distribution that differs considerably from the one in which the total drag is minimized. The wing profile drag contribution can found from :

$$C_{D_v} = \frac{1}{U_\infty^2 S_{ref}} \int_{C_T} C_{d_v} \left(U_\infty + u_p\right)^2 c \, dS \quad (19)$$

The profile drag coefficient can be determined either through the input of two-dimensional airfoil characteristics or alternatively by using empirical relationships like the DatCom-Hoerner rule[9].

The profile drag coefficient is estimated using a quadratic relation :

$$C_{d_v} = f(C_l) = C_{d_0} + f_1 C_l + f_2 C_l^2 \quad (20)$$

with the local lift coefficient being :

$$C_l = \frac{1}{c} \left(\frac{2(U_\infty + u_p)\cos\zeta}{U_\infty^2} \Gamma\right) = \frac{\Gamma'}{c} \quad (21)$$

the viscous drag becomes :

$$C_{D_v} = \frac{1}{U_\infty^2 S_{ref}} \int_{C_T} \left(U_\infty + u_p\right)^2 c \cdot \left(a_0 + a_1 \Gamma + a_2 \Gamma^2\right) dS \quad (22)$$

Optimization formulation

The minimization technique that is used in the program is based on the augmented Lagrange Integral Method. A detailed description is given by van den Dam[11] and Middel[9].

The optimization algorithm minimizes the object function given by :

$$OBJ = C_D + W(C_{L_0} - C_L) \quad (23)$$

in which W is a weighing factor.

In our case the object function including the lift constraint ($C_{L_{des}}$) is defined as :

$$I = C_{D_i} + C_{D_v} + \lambda (C_L - C_{L_{des}}) \quad (24)$$

All parts of this object function can be written in terms of the circulation distribution combined with the unknown Lagrange multipliers λ.

Using the method of variational calculus finally a system of linear equations is found which is solved for the unknown values of the local circulation strength.

Summation over the complete configuration then yields the downwash at all spanwise stations. From these values the total lift coefficient and the total drag coefficients are found :

$$C_{D_i} = \frac{1}{U_\infty^2 S_{ref}} \sum_{i=1}^{n} (v_n(i) + 2(v_p(i) \cdot n_y(i) + w_p(i) \cdot n_z(i)))\Gamma(i)\Delta s(i) \quad (25)$$

Generation of the optimized geometry

After the discussion about the acquisition of the optimum lift distribution for a given propeller/wing combination the logical step is to define how the required distribution can be obtained.
To get some understanding of the magnitude of the changes to an initial wing design, a simple analysis is suggested here.

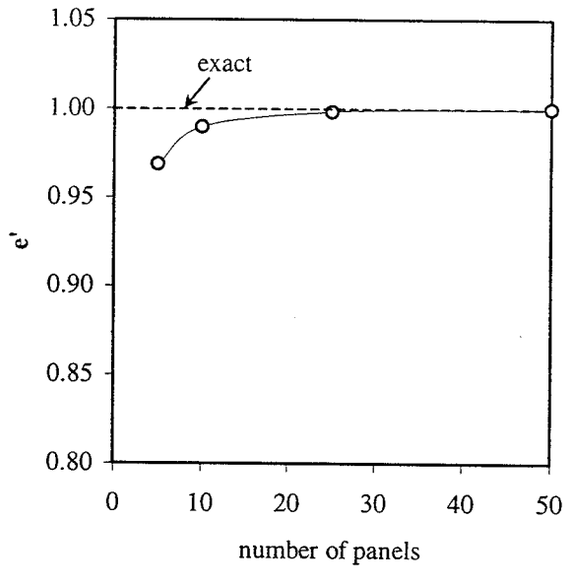

(b)

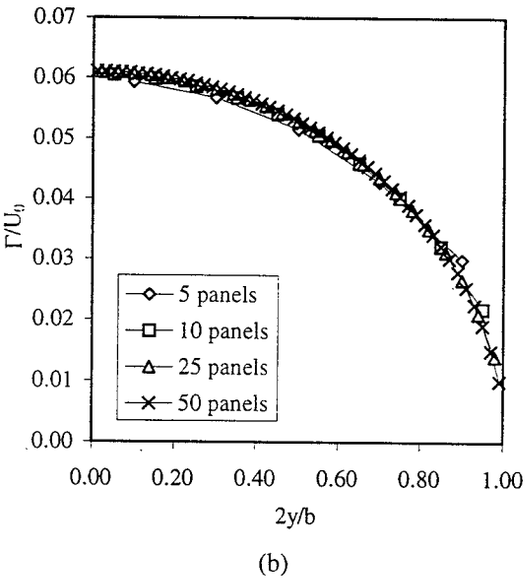

(b)

fig. 3 Accuracy of the induced drag calculation for a planar wing at $C_{L_{des}} = 0.4$, (a) span efficiency factor, (b) change in lift distribution.

From eq. (21) The requirement for the wing now becomes :

$$C_{l_\alpha}(y)(\alpha_g(y) - \alpha_i(y) - \alpha_0(y)) = \frac{\Gamma'}{c}(y) \quad (26)$$

Since the induced angle of attack α_i is fixed by the given vorticity distribution along the span, the user may select one of the following parameters to fulfil the requirement of eq. (26) :

- the 2-dimensional lift curve slope, c_{l_α}
- the geometrical airfoil angle of attack which is determined by the twist distribution, α_g
- the zero lift angle of attack of the airfoil, α_0
- the chord/span ratio of the airfoil

It is clear that the wing design of an optimum wing with installed propeller is complicated due to the difference between the optimum lift distribution and the "normal" elliptic-like distribution, especially at transonic speeds. In general the profile shape should be modified to prevent unwanted viscous and compressibility effects in the part of the wing that is immersed in the slipstream.
Since leading and trailing edge of the wing are normally kept straight and the airfoil type (and camber) will not change strongly in spanwise direction, in general the most attractive way to generate the optimum wing lift distribution may be an adaptation of the twist distribution. Due to deformation of the airfoil shape as a result of wing twist, a combination of twist adaptation and variation of section shape will in practice however be employed.

Induced drag minimization

For a clean wing in absence of a propeller slipstream the optimum loading distribution is elliptically. Thus the circulation distribution can be written as :

$$\Gamma = \Gamma_0 \sqrt{1 - \eta^2} \quad (27)$$

However, this is only true for a flat wake which in practice is never realized.
To check the code some calculation results are presented for a different number of panels. It is clear that increasing the number of panels brings the solution closer to the theoretical elliptical distribution (fig. 3(b))
This can also be seen in fig.3(a) where the span efficiency factor *e* defined as :

$$e = \frac{C_L^2}{\pi A C_{D_i}} \quad (28)$$

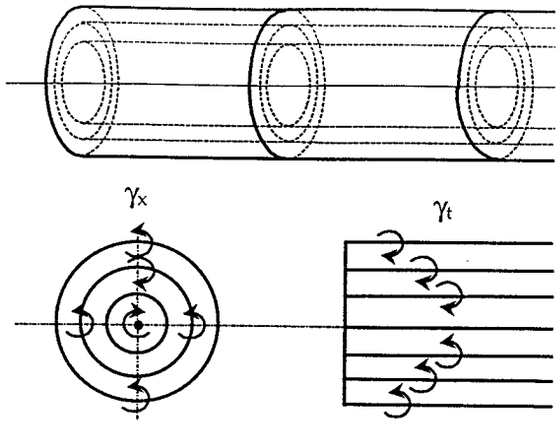

fig. 4 Vortex tube model of the propeller slipstream.

is given.
The solution converges to the theoretical optimum value of 1.0 when more panels are used. With a model containing 25 panels the induced drag is already computed with an accuracy of 0.2 percent.
In the following paragraph the span efficiency factor e will be used to analyze the performance of the propeller wing configuration.

Propeller slipstream

To find the correct interference effect that the slipstream imposes on the wing the axial and the tangential flow velocities, which together form the velocity vector (u_p, v_p, w_p), must be incorporated as given in eq. (16) and eq. (17).
In the current program it is possible to import experimental slipstream data or calculate the propeller induced velocities with a simplified slipstream model. In the latter case (u_p, v_p, w_p) is calculated with the vortex tube model as sketched in fig. 4.
In this model, the vorticity in the slipstream originally concentrated on a finite number of helical vortex sheets, is replaced by two superimposed continuous distributions of vorticity: axial and tangential vorticity :

$$\gamma_x = \frac{B}{2\pi y}\frac{d\Gamma_p}{dy}$$
$$\gamma_t = \frac{nB}{U_\infty}\frac{d\Gamma_p}{dy} \qquad (29)$$

Using a Biot-Savart calculation algorithm the propeller induced velocity vector is then found in the Trefftz plane.

In case the propeller is put at a positive angle of attack to the flow the induced velocity distribution should be given according to the increased values at the down-going blade side and vice versa. If only data are available for the setting $\alpha_p = 0°$ at the position of the propeller plane instead of the wing location, the program will calculate the propwash data according to the following scheme.

axial flow velocity
The axial velocity increase at a certain distance x_p behind the propeller is given by $a_x = v_a/U_0$. According to Smelt & Davies[12] and Durand[13] this can be estimated by :

$$a_x = a\left(1+\frac{1}{\sqrt{(\frac{R}{x_p})^2+1}}\right) \qquad (30)$$

swirl velocity
The flow velocity in the direction of the thrust line is given by $U_\infty \cos(\alpha_p)$ whereas the velocity perpendicular to this line is $U_\infty \sin(\alpha_p)$. The slipstream centerline will therefore deviate from the thrust line, given by the angle :

$$\tan(\alpha_{c.l.}) = \frac{U_0 \sin(\alpha_p)}{U_0(1+a_x)\cos(\alpha_p)} = \frac{\tan(\alpha_p)}{(1+a_x)} \qquad (31)$$

To account for the "upwash effect" given by $\alpha_{c.l.}$ the local swirl velocity at the wing position is corrected through :

$$a_t = \tan(\alpha_w + \alpha_{prop} - \alpha_{c.l.} + \arctan(a_t)) \qquad (32)$$

where $a_t = v_t/U_0$.

Propeller angle of attack

When the direction of the airflow is not perpendicular to the propeller disk, the blades will be subject to alternating loads with a period equal to the time of revolution of the propeller. The correct setting for minimum alternating loads on the blades depends typically on the streamwise position of the propeller with reference to the wing. This can easily be seen from a simple flow model in which the lifting wing is modeled as a single lifting line (fig. 5) with trailing vortices.
The induced flow angles at the propeller plane can simply be calculated using Biot-Savart's rule. In this flow model the effects of the nacelles are neglected although it is clear that they may introduce signifi-

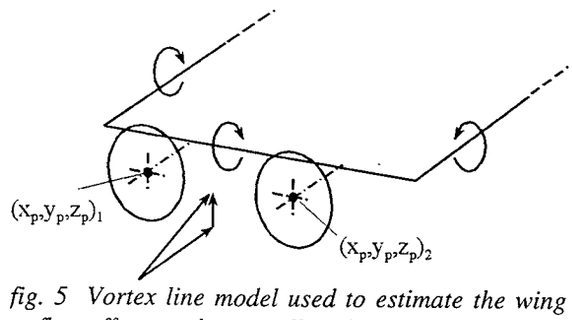

fig. 5 Vortex line model used to estimate the wing upflow effects at the propeller plane.

cant flow non-uniformity. It should be noted that for closely coupled propeller-wing configurations the wing induced angle of attack is substantial. Therefore it should be taken into account when the angle of attack effects on the slipstream velocities are considered. Program *pwopt2* makes use of the given simple flow model to correct the propeller angle of attack for wing induced upflow.

The propeller at angle of attack will, in addition to moments, produce a thrust and a normal force.
The true propeller tilt down-effect on the performance of the propeller/wing configuration is calculated through usage of either an estimated propeller normal force gradient from ESDU[14] or alternatively experimental values when they are available.
Conversion from propeller to wing gives :

$$\frac{dC_{N_w}}{d\alpha_p} = \frac{dC_{N_p}}{d\alpha_p} \cdot \frac{\pi}{4} \frac{D^2}{S_w} = \frac{dC_{N_p}}{d\alpha_p} \cdot g \qquad (33)$$

The primary contributions of the propeller to wing lift and drag are given by :

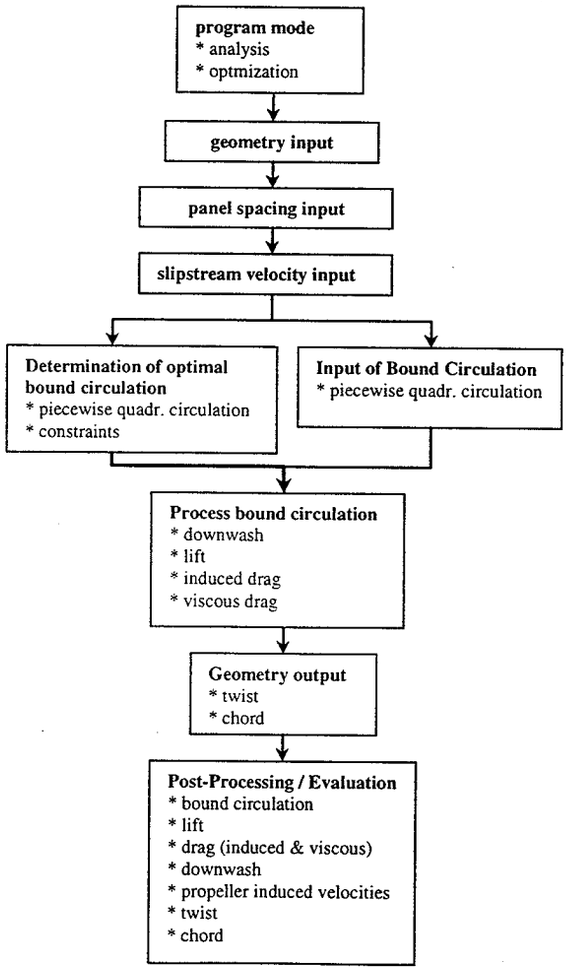

fig. 6 Flow scheme of the optimization program pwopt2.

Parameter	high speed	low speed
density, ρ [kg/m^3]	0.934	0.872
temperature, T [K]	264	261
True airspeed, TAS [m/s]	119.5	75
revolutions per second [Hz]	20	20
blade angle [°]	37.61	33.78
advance ratio	1.633	1.025

Table 1 Flight conditions for the low speed and the high speed case of the Fokker 50.

$$\Delta C_L = (C_{N_p} \cos(\alpha'_p) + T_c \sin(\alpha'_p)) \cdot g$$
$$\Delta C_D = (C_{N_p} \sin(\alpha'_p) - T_c \cos(\alpha'_p)) \cdot g \qquad (34)$$

Where, the propeller geometrical angle α'_p is defined by :

$$\alpha'_p = \alpha_p + \alpha_w \qquad (35)$$

The complete flow scheme of the program in which the optimization algorithms are implemented is presented in fig. 6.

Calculation results

Optimization of a tractor propeller wing configuration

To investigate the propeller slipstream effect on the wing performance a configuration similar to that of the Fokker 50 was selected (fig. 7).
Two typical cases were investigated : the so-called "high speed case" and the "low speed case" (table 1).
The slipstream data for these cases, that were taken from Janssen[15], are symmetrical with resect to the propeller axis; i.e. the propeller is positioned perpendicular to the local flow. Hence the upflow in front of the wing is compensated for.

First the effect of the rotation direction on the optimal lift distribution was investigated. In fact three different cases were examined :

- inboard up rotating propellers
- outboard up rotating propellers
- co-rotating propellers

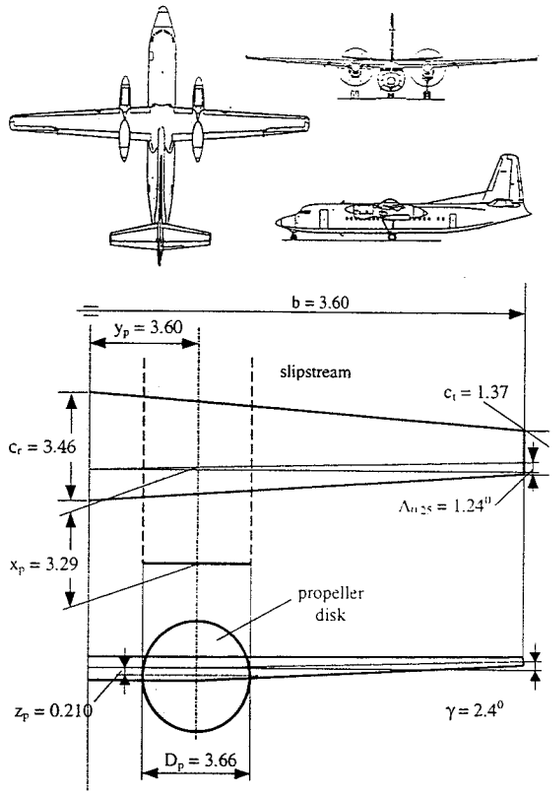

fig. 7 Fokker F50 configuration investigated in the optimization process.

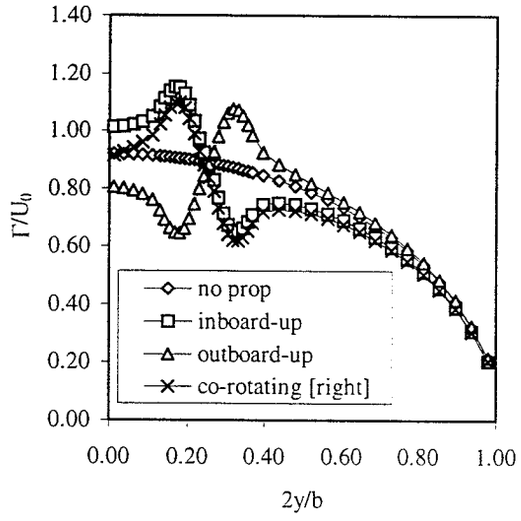

fig. 10 Optimal spanwise bound circulation distribution for different rotation directions ; $C_{L_{des}} = 0.6$

The optimum bound circulation distribution given in fig. 10 differs significantly from the elliptical clean wing configuration due to the action of the propeller. The local circulation strength shows a jump going from the inboard to the outboard side of the wing. This could expected since the magnitude of the lift vector tilted forward is bigger than the one tilted backward. The propeller produces both positive and negative contributions to the spanwise induced drag

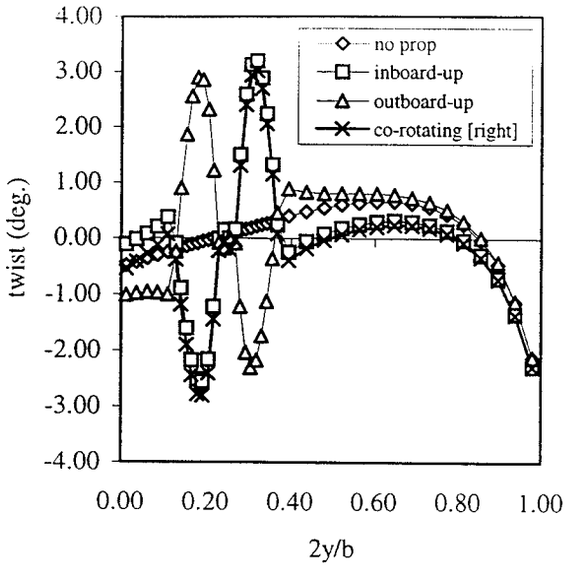

fig. 8 Optimal twist distribution for different directions of rotation at $C_{L_{des}} = 0.6$

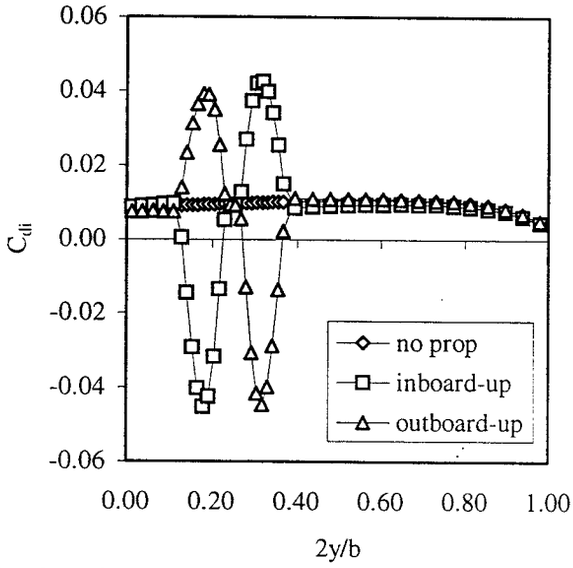

fig. 9 Induced drag distribution for different directions of rotation at $C_{L_{des}} = 0.6$

(fig. 9). The negative contribution at the upgoing blade (UBS) side exceeds the positive contribution at the downgoing blade side (DBS) resulting in the reduction of the overall induced drag.

As described in eq. (26) the sectional shape can now be changed to realize the optimum lift distribution. In fig. 8 the optimum twist distribution is presented when the local chord and airfoil shape are left unaltered. The resulting maximum twist angle is about 3.5°. Changing the local chord with unchanged twist distribution produces unrealistic chord values (see fig. *11*). hence twist and camber adaptation seem to be the only acceptable design variables.

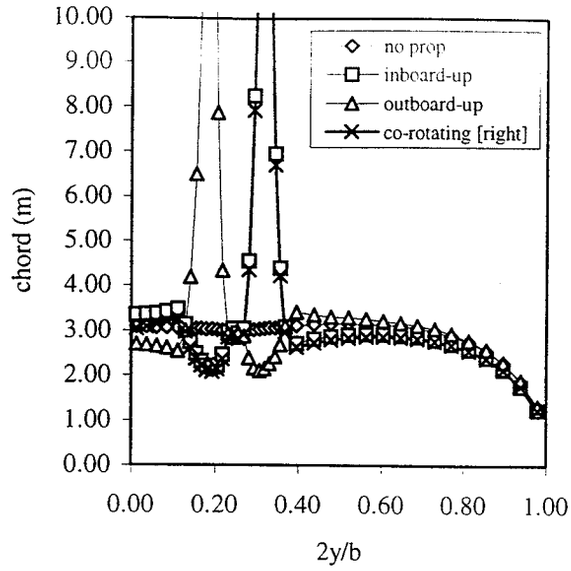

fig. 11 Optimal chord distribution with standard twist distribution of the F50-wing at $C_{L_{des}} = 0.6$.

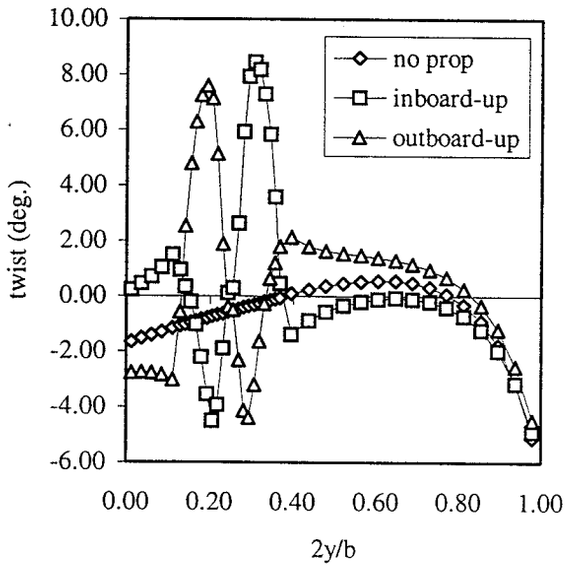

fig. 12 Optimal twist distribution for different rotations directions at $C_{L_{des}} = 1.2$

The results of the optimization process for the low speed case are presented in fig. 8 .
The magnitude of the slipstream velocities has increased. This makes the results somewhat less accurate since in the Trefftz plane analysis the perturbation velocities were assumed to be small. Of course the shape of the optimum circulation differs from the high speed case. This signifies that the wing can only be optimized for a specified flight condition (generally cruise).
Due to the higher slipstream velocities the wing induced drag reduction in the low speed case is larger ($\Delta C_{D_i} = -60$ counts) than for the high speed case ($\Delta C_{D_i} = -10$ counts).

Propeller at angle of attack

As indicated by experiments on a generic propeller/wing model, performed earlier by van Es[16], the wing performance may significantly be influenced by the propeller angle of attack with respect to the wing reference chord line. The so-called PTD-configuration (propeller-tilt-down) used by Veldhuis[3] suggests a reduction of overall wing induced drag. This effect of the propeller angle of attack was investigated again for the given F50-like configuration. The normal force gradient of the six-bladed propeller was taken from windtunnel tests on a generic propeller-wing model (APERT-JR01); data of which were published by Kusomo et al.[17].

To express the performance of the propeller-wing configuration incorporating the direct forces acting on the propeller we use :

$$T'_{c_{eff}} = -\left(C_{D_i} + \Delta C_{D_p} - \Delta C_{D_i} \right) \tag{36}$$

with :

$$\Delta C_{D_i} = (C_{D_i})_{no\ prop} - (C_{D_i})_{with\ prop} = \frac{2C_L^2 \cdot \Delta C_{L_p} + \Delta C_{L_p}^2}{\pi A e} \tag{37}$$

where index p denotes the effect due to the propeller. Here the profile drag is ignored in the optimization process.
Fig. 13 and 15 show the effect of propeller angle of attack on the wing efficiency. The highest "effective

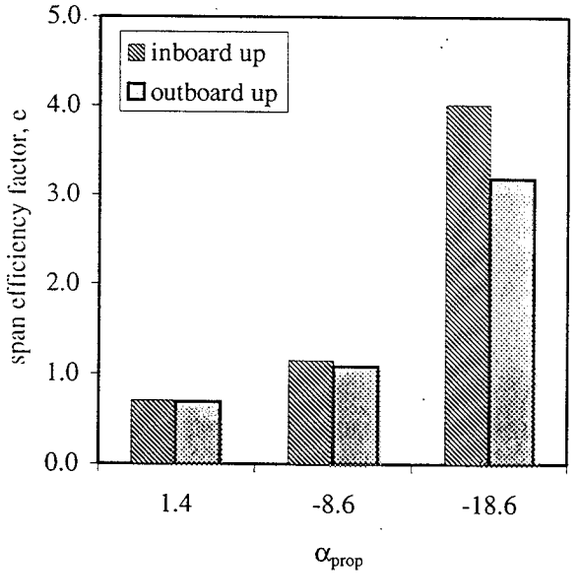

fig. 13 Effect of propeller angle of attack on the wing span efficiency factor e.

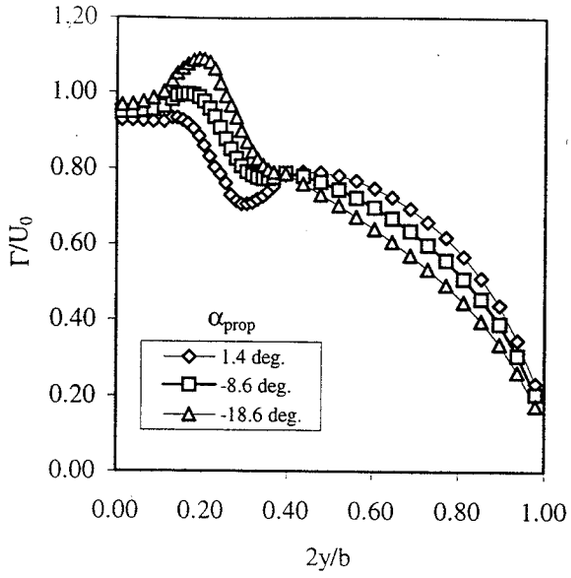

fig. 14 Optimum lift distribution for different propeller angles of attack.

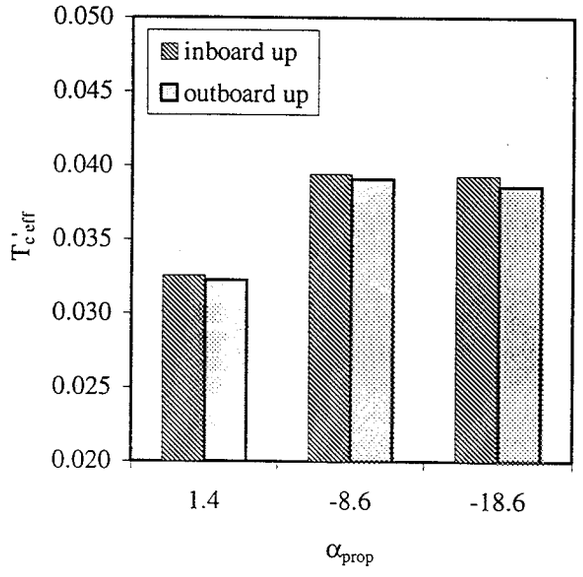

fig. 15 Propeller angle of attack effect on the "effective thrust coefficient" of the configuration.

thrust" is found at relatively large negative angles of attack (fig. 15). Apparently the benefits of the wing drag reduction due to the presence of the propeller increase with negative propeller-angle of attack, α_p.

It should be remarked that, in contrast with what one would expect, the reduction of wing lift and effective thrust, through direct forces acting on the propeller, are smaller than the benefits in the sense of reduction of the overall induced drag.

The phenomenon sketched above can be explained as follows. When α_p becomes more negative the local blade angle of attack of the downgoing blade increases while that of the upgoing blade becomes smaller. This results in an asymmetrical slipstream. Since the lift vector at the side of higher local lift coefficient is tilted forward and the lift vector at the other side is tilted backward a net drag reduction remains. Accordingly, a swirl velocity distribution with lower values at the DBS and higher values at the UBS should increase the wing efficiency factor.

Besides this the whole slipstream will be placed at an angle which attenuates the forward tilting process (resulting in increased leading edge suction) at both sides of the nacelle. Again the configurations with inboard up rotating propellers demonstrate a superior performance compared to the outboard up rotating cases. In fig. 14 the optimum lift distribution is presented for several propeller angles of attack . Apparently the propeller angle of attack strongly influences the form of the optimum lift distribution.

An inevitable disadvantage of a configuration with negative propeller angle of attack (PTD) is of course the emergence of cyclic blade loading.

The resulting variation in blade stresses with azimuthal position and the possible increase in noise level are problems to be addressed before a PTD-configuration can be practically implemented.

Effect of profile drag

To investigate the effect of the profile drag on the optimum wing loading distribution NACA 64_2A015 airfoil were used. At low lift coefficients, between *-0.3* and *0.3*, the c_{l_α} -curve is rather flat. This means that an optimization with a constrained value in that lift range will hardly result in a changed optimal lift distribution.

In fig. 19 and table 3 the optimization result with and without the profile drag contribution of a simple rectangular wing of low aspect ratio(A=*5.3*) is given.

This wing was used during experiments by van Es[16].

Here the constrained value of the design lift coefficient is equal to *0.9* to demonstrate the influence of the profile drag into the optimization results.

When both drag contributors are used in the optimization process, there is only a minor change in the lift distribution. This agrees with the result of Middel[9].

The total values of the drag coefficients of the wing are given in table 3 for both the inboard-up as well as the outboard-up rotating propeller. Although the differences are small for the current testcase, it can be seen that for the inboard-up rotating propeller the induced drag is greater when the sum of the induced drag and the profile drag is minimized than when the induced drag alone is optimized. However, the profile drag has become smaller towards a more optimized value. The total drag, as a result of the optimization of the sum of the induced and viscous drag, is less than it would have been if only the induced drag was minimized and the viscous drag was added afterward.

Con-figu-ration	Mini-miza-tion	C_{D_i}	C_{D_p}	$C_{D_{tot}}$
inb. up	i	0.043711	0.010669	0.054380
inb. up	i + v	0.043732	0.010642	0.054374
outb. up	i	0.046287	0.010531	0.059819
outb. up	i + v	0.046299	0.010520	0.056819

i=induced drag, v=viscous drag

Table 3 Influence of the profile drag distribution on the wing drag coefficient of a low aspect ratio wing at $C_{L_{des}} = 0.9$ (van Es(16))

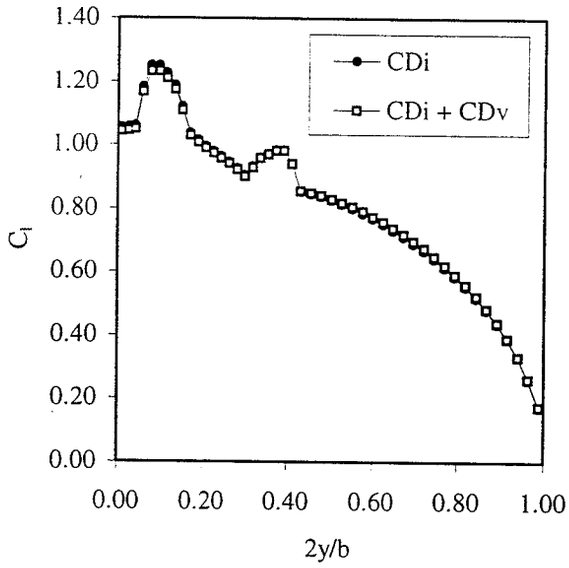

fig. 19 Optimum lift distribution with and without usage of viscous drag in the optimization process.

Comparison of optimization and analysis.

The performance of the optimized propeller-wing configuration was further analyzed with a higher order Panel Method *FASD*[18].

Initial design		
Configuration	C_L	C_{Di}
No propeller	0.598	0.0101
Inboard-up	0.599	0.0088
Outboard-up	0.600	0.0093
Optimized design		
Configuration	C_L	C_{Di}
No propeller	0.599	0.0091
Inboard-up	0.599	0.0078
Outboard-up	0.600	0.0083

Table 2 Effect of the optimization on the wing drag coefficients at $C_{L_{des}} = 0.6$; high speed case.

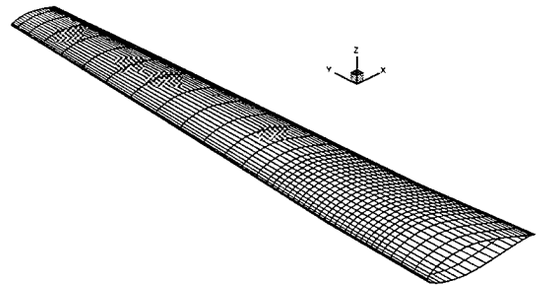

fig. 16 Higher order panel models of the initial geometry without nacelle.

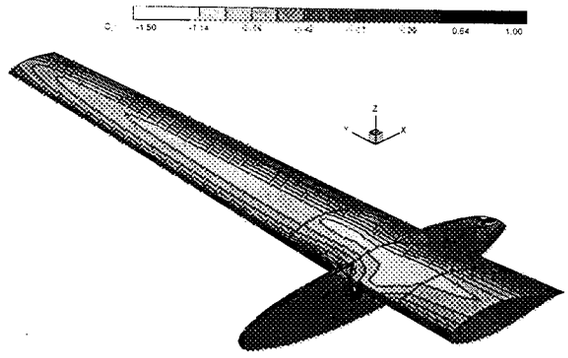

fig. 17 Panel model with pressure distribution at the upper side of the initial geometry under influence of an inboard-up rotating propeller at $M = 0.35$

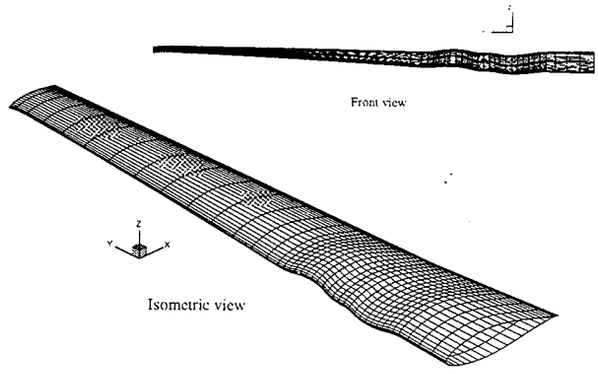

fig. 18 Panel model of the optimized geometry of the wing configuration at $C_{L_{des}} = 0.6$. Optimized for inboard-up rotation.

Here only the contra-rotating propeller case was calculated with the same slipstream input as used in the optimization process.
The high speed case was calculated as $M = 0.35$ and $C_L = 0.6$ while the low speed case was run at $M = 0.22$ and $C_L = 1.2$.
In fig. 16 and fig. 17 the initial panel geometry is presented. When the wing geometry is adapted ac-

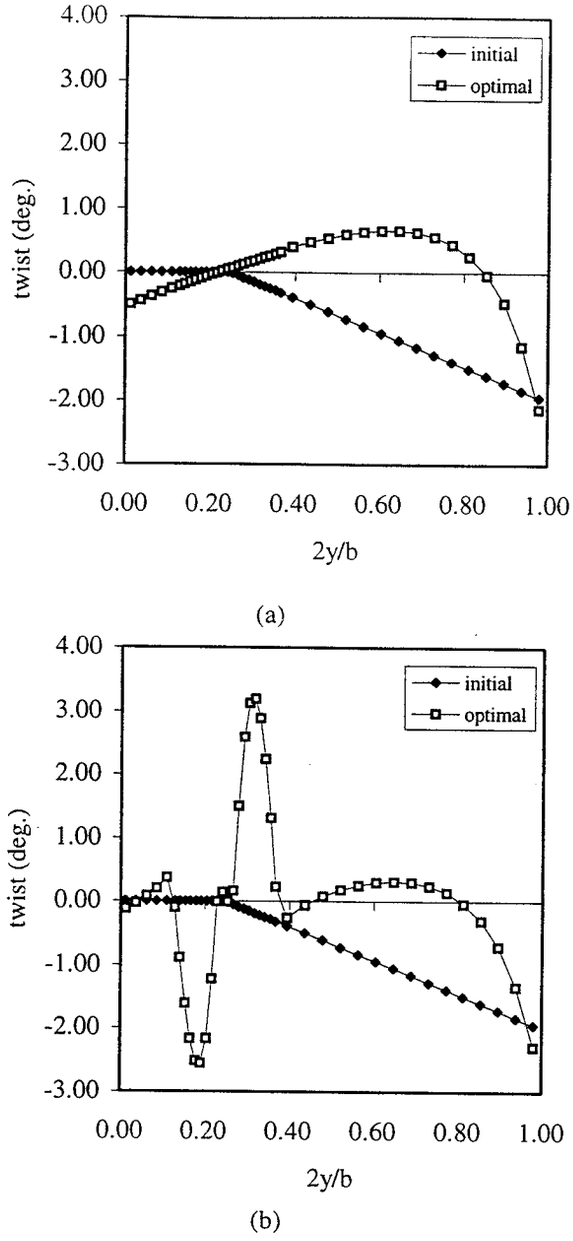

fig. 20 Twist distribution of the initial and optimized wing at $C_{L_{des}} = 0.6$; high speed case; (a) prop-off, (b) inboard up rotation.

cording to the optimum twist distribution (see fig. *20* and fig. *18*) found earlier the resulting the induced drag is indeed reduced as can be seen in table *2*.
Although the effects for the symmetrical slipstream that was used here are very small.
As can be seen, the wing twist is mainly affected in the area washed by the propeller slipstream.

Conclusions

From the current analysis the following conclusions may be drawn :

- A simple and fast optimization program for the optimization of propeller-wing configurations in the preliminary design phase was developed which enables investigations of the effects of : propeller position, slipstream velocity distribution and adaptations to conventional wing designs.
- Calculations show that the propeller-wing configuration benefits from a relatively large negative propeller angle of attack (PTD-configuration). This effect is mainly due to the asymmetry in the slipstream velocity distribution that is introduced. However in an analysis including viscous effects in high subsonic flow there will be a maximum in the attainable effective efficiency since drag rise with Mach number and separation effects may nullify the local leading edge suction.
- It is shown that the inboard-up rotating propeller exhibits a superior performance compared to the conventional co-rotating or the outboard-up rotating case. Therefore further investigation of this configuration to arrive at a practical implementation is recommended.

References

1. Kroo, I : "Propeller / wing integration for minimum induced loss", J. of Aircraft , July 1986, Vol. 23 , No. 7 , p. 561-565

2. Miranda, L.R. ; Brennan, J.E. : "Aerodynamic effects of wing tip mounted propellers and turbines", AIAA 86-1802 , 1986, p. 221-228

3. Veldhuis, L.L.M., "Experimental Analysis of Tractor Propeller Effects on a Low Aspect Ratio Semi-Span Wing", Second Pacific International Conference on Aerospace Science and Technology & the Sixth Australian Aeronautical Conference, Vol. 2, p. 491-498, Melbourne, 20-23 march 1995.

4. Kuhlman, J.M. : "Higher order Farfield Drag Minimization for a subcritical Wing Design Code", Journal of Aircraft, vol. 17, No.9, 1980

5. Heyma, P.M. : "Analysis and Optimization of a Tractor Propeller-wing configuration", TWAIO-thesis, June 1996, Dept. of Aerospace Engineering, Delft University of Technology

6. Veldhuis, L.L.M. : "Experimental analysis of the vortex wake structure behind a propeller-wing configuration", AGARD-CP-584, Conf. proceedings 584, 1996, AGARD Symposium , Trondheim Norway

7. Lötstedt, P. : "Accuracy of a propeller model in inviscid flow", Journal of Aircraft, vol. 32, No. 6, nov./dec. 1995

8. Colin, P. ; Moreux, V. ; Barillier, A. : "Numerical study of high speed propeller engine integration on transport aircraft", ICAS-96-4.10.1, Sorrento Italy, Sept. 1996

9. Middel, J. : "Development of a computer aided toolbox for aerodynamic design of aircraft at subcritical conditions with application to three-surface and canard aircraft, Dissertation,1992, Delft University Press"

10. Munk, M.M. : "The minmum induced drag of aerofoils", NACA Report 121, 1921

11. Dam, R.F. van den : "Samid, an interactive system for aircraft drag minimization ; Mathematical models and methods", NLR TR 880714, 1998

12. Smelt, R. ; Davies, H. : "Estimation of increase in lift due to a slipstream", ARC R&M 1788, 1937

13. Durand, W.F. : "Aerodynamic Theory", 1935, Volume IV, Divisions J-M, Springer Verlag, p. 169-430

14. ESDU : "In-plane forces and moments of installed propellers at low speeds", ESDU 89047, 1989, ISBN 0 085679 721-9, ESDU International plc.

15. Janssen, M.
"An evaluation of methods for the calculation of the flow around propeller at angle of attack", M.Sc Thesis, 1991, Dept. of Aerospace Engineering, Delft University of Technology

16. Es, G.W. van : "Experimental investigation of the effect of propeller angle of attack and position on the aerodynamic characteristics of a tractor-propeller wing combination"
thesis, 1993, Dept. of Aerospace Engineering , Delft University of Technology

17. Prijo Kusumo, J. ; Gayus, L.G.M. ; Custers, L.G.M. ; de Haij, L.H. ; Veldhuis, L.L.M. : "Experimental investigation on propeller slipstream effects on a swept wing at low speeds", ICAS-96-4.10.2, Sorrento Italy, Sept. 1996

18. Hoeijmakers. H.W.M. , Bosse, S. : Private communications